ACS APPLIED POLYMER MATERIALS

pubs.acs.org/acsapm Article

Engineering Three-Dimensional Morphologies in a Block Copolymer by Reversible Metal Infiltration

Mingchao Ma and Caroline A. Ross*

Cite This: https://doi.org/10.1021/acsapm.4c02331 Read Online

ACCESS | Metrics & More | Article Recommendations | Supporting Information

ABSTRACT: A range of three-dimensional (3D) morphologies is established in layered thin films of a block copolymer, polystyrene-*block*-poly(2-vinylpyridine) (PS-*b*-P2VP) (115 kg/mol, P2VP volume fraction 31.6%), by combinations of spin coating, solvent annealing, reversible metal infiltration, and surface modification by oxygen etching. Pt infiltrated into the cylindrical-morphology P2VP blocks from an acid solution containing $[PtCl_4]^{2-}$ locks the morphology of the bottom layer during the coating and annealing of a second layer, leading to a range of bilayered and trilayered 3D structures, including in-plane orthogonal meshes and layered I-shape and inverted T-shape P2VP microdomains. In contrast, unloading the metal by a KOH plus ethylenediaminetetraacetic acid disodium salt dihydrate (Na_2EDTA) solution allows chain reorganization during subsequent layer coating and annealing, producing morphologies characteristic of a single layer of the PS-*b*-P2VP. However, a short oxygen etch modifies the surface, impedes chain reorganization, and yields multilayer structures even when the metal unloading process is performed. Metal infiltration and exfiltration combined with layering, annealing, and oxygen etching diversify the morphologies available from the block copolymer and provide a path to localized morphology control, expanding the toolkit for 3D nanofabrication.

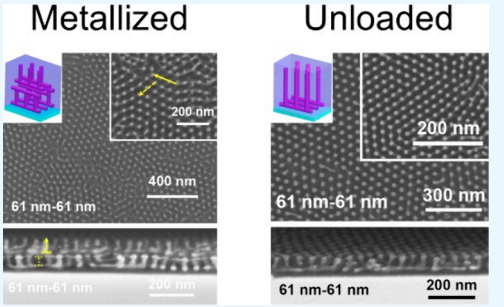

KEYWORDS: *self-assembly, block copolymer, 3D morphology, metal infiltration, metal exfiltration*

INTRODUCTION

Block copolymers (BCPs) can form various periodic morphologies by self-assembly, including lamellae, gyroids, hexagonally packed cylinders, or spheres, making them useful for nanofabrication and pattern transfer.[1−4] BCPs are characterized by the degree of polymerization (N), the Flory−Huggins interaction parameter (χ), and the block volume fraction (f),[5−7] which determine the equilibrium bulk microdomain morphology. For BCP thin films, the morphologies can be further modified via processing parameters, including the surface or interface chemistry,[8−10] solvent annealing,[11−14] flash lamp annealing,[15,16] film thickness,[17−19] or patterning the substrate to provide a template for self-assembly.[20−22] For example, in films of PS-*b*-P2VP,[18] polystyrene-*b*-poly(methyl methacrylate) (PS-*b*-PMMA),[17] and polystyrene-*b*-poly(dimethylsiloxane) (PS-*b*-PDMS),[19] increasing thickness promoted reorientation of cylindrical microdomains from in-plane to out-of-plane.

Much of the work on BCP-based nanofabrication has made use of films with 2D self-assembled structures, e.g., vertical cylinders or lamellae, or single layers of in-plane cylinders or spheres, where there is little structural complexity in the out-of-plane direction.[23−26] Obtaining custom 3D morphologies with specific out-of-plane microdomain geometries widens the opportunities for BCP-derived nanofabrication, for example, enabling the fabrication of porous channels for photovoltaic devices[27−31] or cross-point structures for microelectronics.[4,26]

One strategy for creating films with 3D structural complexity is layer-by-layer stacking of 2D films, i.e., forming a bottom layer with one morphology, locking the structure by various cross-linking or etching methods, and then coating and annealing an upper layer with a different morphology.[32−35] Locking of the first layer prevents disruption of its morphology during the processing of the next layer. Examples include alternating lamellar and cylindrical microdomains formed in stacked PS-*b*-PMMA thin films after cross-linking the bottom layer by UV irradiation[32,33] and films of polystyrene-*block*-poly(4-vinylpyridine) (PS-*b*-P4VP) that were cross-linked at the surface by physical collisions of ions from an Ar plasma prior to coating a second layer.[34]

Metal infiltration, in which pyridine-containing blocks bind with metal precursors, locks the self-assembled structures and leaves metal patterns after etching,[36−39] making it a useful process in the formation of 3D nanostructures. Pyridine groups

Received: July 25, 2024
Revised: August 28, 2024
Accepted: September 2, 2024

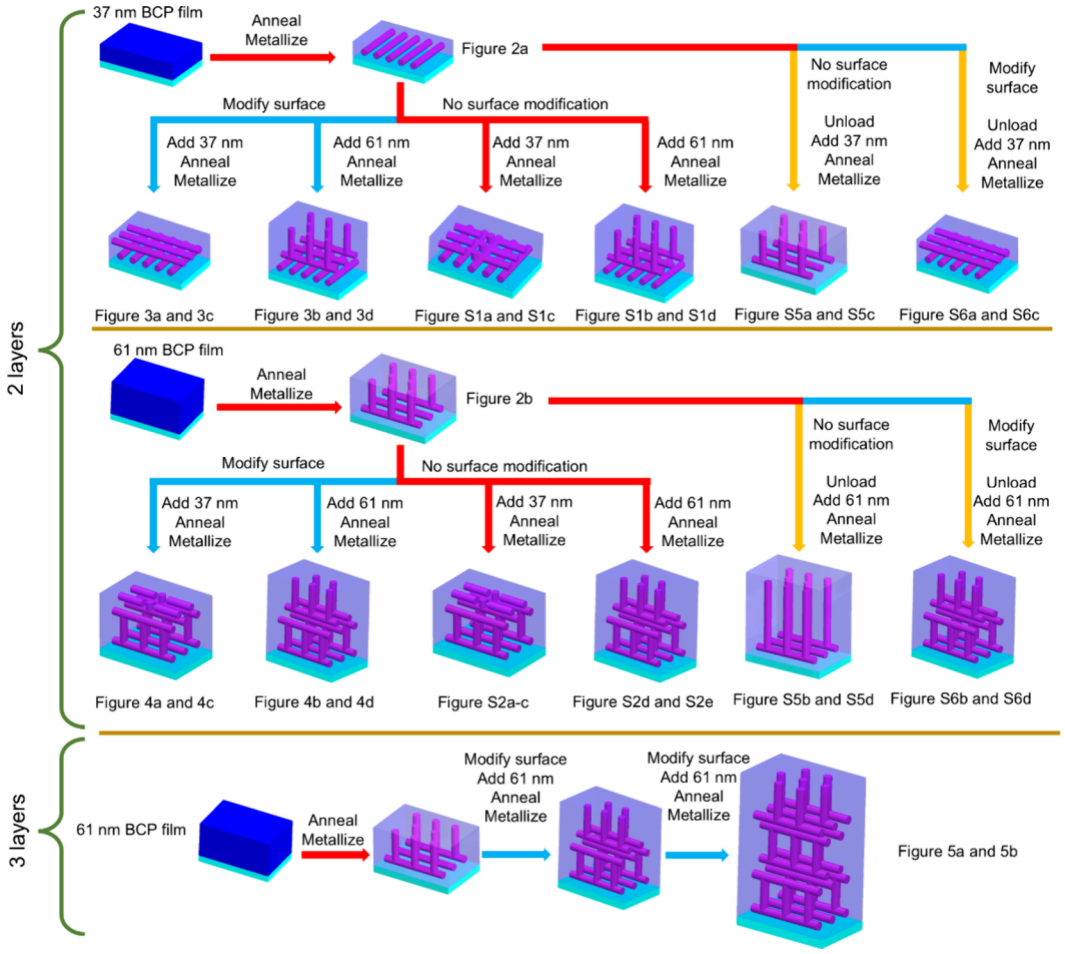

Figure 1. Schematic illustration of constructing 3D structures in a PS-*b*-P2VP thin film. Dark blue represents the disordered film, light blue represents the substrate, purple cylinders indicate the metallized P2VP blocks, and light purple indicates the PS matrix.

accept protons in an acid environment and then bind with anionic metal complexes such as $[PtCl_4]^{2-}$ via an electrostatic interaction,[40−43] introducing metal selectively into the block. P2VP and P4VP blocks have been used as hosts for metal infiltration, enabling construction of 3D nanostructures.[44−47] For example, multicomponent 3D meshes[46] or hierarchical dot/line patterns[47] were formed via sequential metallization and etching of stacked PS-*b*-P2VP or PS-*b*-P4VP thin films.

Exfiltrating metal from metallized BCPs unlocks the structures, allowing the BCP to reorganize in a subsequent annealing process or to be infiltrated by another metal.[43,48] Mun et al. unloaded $[PtCl_4]^{2-}$ from specific regions of PS-*b*-P2VP thin films using aqueous HCl solution and reloaded the P2VP blocks with $[AuCl_4]^-$ to form multicomponent Au/Pt metal patterns.[48] We previously reported that unloading $[PtCl_4]^{2-}$ or $[Fe(CN)_6]^{3-}$ by a KOH + Na_2EDTA complexing solution unlocked the 2D structures in PS-*b*-P2VP thin films and allowed the morphology to change in a subsequent annealing process, which enabled reversible morphology transitions in single-layer films.[43]

Here, we extend this technique to produce unconventional 3D morphologies in stacked PS-*b*-P2VP thin films via metal infiltration using $[PtCl_4]^{2-}$ and metal exfiltration using a KOH + Na_2EDTA solution. Combinations of infiltration, exfiltration, reactive ion etching, and solvent annealing processes in bilayer and trilayer PS-*b*-P2VP yield a range of structures such as stacks of I- and T-shaped morphologies by reorientation of the tips of vertical cylinders. The morphological control enabled by metallization diversifies the applications of self-assembly for nanofabrication.

EXPERIMENTAL METHODS

Materials. The PS-*b*-P2VP BCP, which has a number-average molecular weight (M_n) of 79.0 and 36.5 kg/mol for the PS and P2VP blocks, respectively, was purchased from Polymer Source Inc. The material is designated as SV115 and has a polydispersity of 1.05 and P2VP volume fraction of 31.6%. The BCP was dissolved in toluene to prepare 1 and 1.5 wt % solutions. Na_2PtCl_4 was purchased from Sigma-Aldrich and served as the metal precursor. 10 mM metal precursor was dissolved in 9 wt % HCl aqueous solution to form the metallization solution. A mixed aqueous solution of KOH (0.05 wt %, purchased from EMD Chemicals Inc.) and Na_2EDTA (0.5 wt %, purchased from Sigma-Aldrich) was used as the unloading solution.

BCP Film Preparation. The set of processes used to make 2-layer and 3-layer structures is shown in Figure 1. BCP solutions were spin-coated on silicon wafers with native oxide at 3k rpm (1 wt % solution), producing a film thickness of 37 ± 2 nm, and 2k rpm (1.5 wt %), forming a 61 ± 4 nm film. Two- or three-layer films were constructed by repeating the single-layer preparation process two or three times. The stacked films with different thickness are denoted as *x* nm−*y* nm−*z* nm, where *x*, *y*, and *z* (if present) are the thicknesses of first layer, second layer, and third layer, respectively.

Annealing. The thin films were annealed in a 5 cm diameter × 5 cm height cylindrical glass chamber containing 1 mL of chloroform solvent with 7 sccm nitrogen gas flow for 15 min, reaching a swelling ratio (the ratio of swelled thickness to as-coated thickness) of 2.8. The

https://doi.org/10.1021/acsapm.4c02331
ACS Appl. Polym. Mater. XXXX, XXX, XXX−XXX

solubility parameters for chloroform, PS, and P2VP are 18.9,[49] 18.4,[49] and 21.2 $MPa^{1/2}$,[50] respectively, implying that the chloroform vapor is PS-selective and will swell the PS block preferentially.

Metallization. To infiltrate Pt into the SV115 structure, the metallization solution was dripped on the annealed films and held for 60 min at room temperature and then washed off using deionized water. To unload the metal, the KOH + Na_2EDTA was dripped onto the film and left for 30 min then washed off by deionized water.

Etching. Oxygen plasma etching was carried out using a Plasma-therm 790 reactive ion etching (RIE) system with 6 mTorr pressure, 10 sccm gas flow, and 90 W power. Surface modification (Supporting Information Section 6) was carried out by oxygen etching for 3 s to remove the mushroom-like protrusions of the metallized vinylpyridine block on the surface.[36,41,43] Longer oxygen etches up to 60 s were used to remove organic components and convert Pt-infiltrated P2VP microdomains to metal patterns for visualization by scanning electron microscopy (SEM).

Characterization. A Zeiss Sigma HD VP SEM and a Zeiss Gemini 450 SEM were used to image the self-assembled morphologies. A Bruker Dimension Icon atomic force microscope (AFM) was used to scan the topography of thin films, and a Physical Electronics Versaprobe II X-ray photoelectron spectrometer (XPS) was used to analyze the elemental composition of the surface.

RESULTS AND DISCUSSION

Single-Layer Film. The microdomain morphology of SV115 depends on its thickness and solvent annealing conditions. We previously showed that 37 nm thick films of SV115 annealed in chloroform form a single layer of in-plane P2VP cylinders with a periodicity of 50 nm (Figure 2a, where

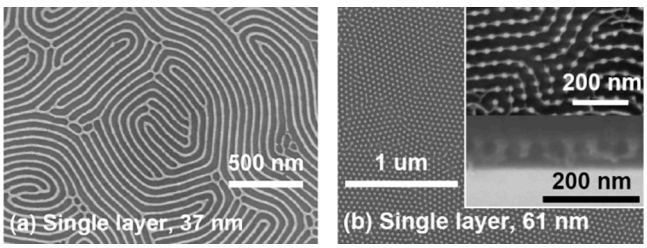

Figure 2. Morphology of single-layer SV115 thin films. The films are prepared by spin coating a layer 37 or 61 nm thick then annealing, metallization, and etching. (a) 37 nm thick film with in-plane cylinders of period 50 nm and (b) 61 nm thick film showing out-of-plane cylinders at the top surface. Insets in (b) show the top view and cross section of the same sample after longer etching, revealing a layer of in-plane cylinders at the bottom of the 61 nm thick film connecting the bases of the out-of-plane cylinders to form inverted-T structures.

the morphology of the Pt-infiltrated P2VP is revealed by reactive ion etching in oxygen).[43] The formation of in-plane cylinders is attributed to the dominant effects of surface and interface energy, which favor PS at the film−substrate and film−air interface and embedded P2VP microdomains parallel to the surface. Mushroom-like protrusions of height 1.8−4.0 nm (Figure S7b) formed on the surface above the cylindrical microdomains after infiltrating the metal, which has been explained as a result of the swelling of P2VP blocks in acid.[36,41,43] These protrusions are removed by the surface modification process (3 s oxygen etch),[36,41,43] which also removes some of the organic blocks and increases the oxygen content at the surface (Figure S8 and Table S1).

As the film thickness increases, the P2VP cylinders reorient to the out-of-plane direction. 61 nm thick films form inverted-T structures (Figure 2b), consisting of a layer of in-plane cylinders adjacent to the substrate, from which perpendicular cylinders emerge. We reported a similar structure for 200 and 485 nm thick SV115, consisting of 1−2 layers of in-plane cylinders adjacent to the substrate transitioning to an out-of-plane orientation throughout the rest of the film.[18] The reorientation is attributed to the gradient of solvent concentration through the film thickness.[18,19,51] In our 61 nm thick films, the perpendicular P2VP cylinders protrude above the PS surface by 2−3 nm after metal infiltration (Figure S7c,d). The surface modification process increases the protrusion of the perpendicular metallized cylinders to 5−8 nm.

Stacked Films. We now demonstrate how stacking 37 and 61 nm thick films can lead to a range of two-layer morphologies shown schematically in Figure 1. We start with examples in which the first layer is a 37 nm thick film. The first layer is metallized and the surface is modified by a 3 s oxygen etch step; then a second layer of 37 or 61 nm thickness is deposited on top, annealed, and metallized (Figure 3). The first layer retains its in-plane cylinder morphology for both thicknesses of the second layer.

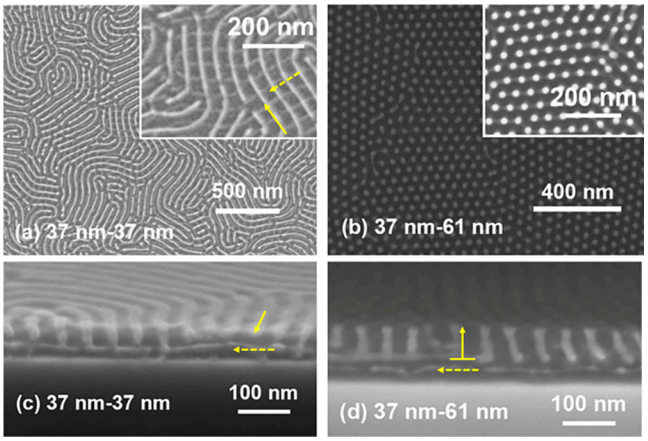

Figure 3. Morphology of two-layer metallized films prepared by spin coating a 37 nm layer of SV115 and then annealing, metallization, and a 3 s surface modification etch, followed by coating a second layer of 37 or 61 nm then annealing and metallization. (a) 37 nm−37 nm top view, (b) 37 nm−61 nm top view with an inset revealing the in-plane cylinders of the upper layer after a longer etching time, (c) 37 nm−37 nm cross section, and (d) 37 nm−61 nm cross section. Dashed arrows indicate the bottom layer of in-plane cylinders, and solid arrows indicate the upper layer cylinders.

When the second layer is 37 nm thick, it forms in-plane cylinders preferentially oriented orthogonal to the bottom layer of cylinders (Figure 3a,c), yielding mesh structures analogous to those produced by both PS-*b*-P2VP and PS-*b*-PDMS bilayers in prior work.[46,52,53] Omitting the surface modification step before coating the 37 nm second layer results in a mixture of in-plane and out-of-plane cylinders in the upper layer, with less preference for orthogonal arrangement (Figure S1a,c). This is most likely a result of the protrusions formed by metallization[36,41,43] (Figure S7b) degrading the quality of the ordering of the second layer.

If the second layer is 61 nm thick, an inverted-T morphology consisting of in-plane cylinders connected to vertical cylinders is formed above the lower layer of in-plane cylinders (Figure 3b,d).[18] Omitting the surface modification step yields the same morphology, though the first layer of in-plane cylinders appears thicker (Figure S1b,d).

https://doi.org/10.1021/acsapm.4c02331
ACS Appl. Polym. Mater. XXXX, XXX, XXX−XXX

We now consider cases where the first layer is 61 nm thick, annealed, metallized, and treated with a surface modification etch. The first layer exhibits inverted T structures. A second layer of 37 nm thickness exhibits a majority of in-plane cylinders with some out-of-plane cylinders (Figure 4a,c). Most

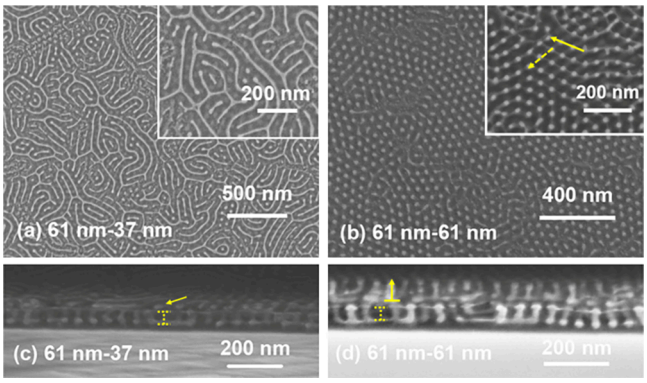

Figure 4. Morphology of two-layer metallized films. The films are prepared by spin coating a 61 nm layer of SV115 and then annealing, metallization, and surface modification, followed by coating a second layer of 37 or 61 nm then annealing and metallization. (a) 61 nm−37 nm top view, (b) 61 nm−61 nm top view with insets showing the structure after a longer etching time, (c) 61 nm−37 nm cross section, and (d) 61 nm−61 nm cross section. Dashed arrows indicate the cylinders of the first layer, and solid arrows indicate the second layer cylinders.

of the in-plane cylinders from the second layer lie between the tops of the vertical cylinders of the first layer, but some lie directly above the vertical cylinders. (A similar morphology is produced if the surface modification step is omitted before coating the second layer; Figure S2a−c.) In the cross section (Figures 4c and S2d) we see that the first layer morphology has been modified by addition of the second layer. A bridging layer formed across the top of the vertical cylinders, converting the inverted-T into an I-shaped cross section. Above this we observe the in-plane cylinders of the 37 nm thick second layer.

Figure S2b,c further reveals the underlying morphology of the 61 nm thick first layer by removing the second layer using 60 s etching: we observe in-plane cylinders at the bottom of the lower layer with vertical cylinders emerging from them, and fragments of the cylinders of the top layer remain. Hence the 61 nm−37 nm film consists of I-shaped structures from the first layer surmounted by in-plane cylinders from the second layer.

Next, we describe the 61 nm−61 nm structure shown in Figure 4b,d, prepared with a surface modification step before the second layer. The lower layer produced an I-shaped structure similar to that seen in the 61 nm−37 nm sample, and the upper layer forms an inverted-T structure. Without the surface modification step (Figure S2e,f), the morphology is similar, but the vertical cylinders of the upper layer are less uniformly oriented in the out-of-plane direction.

Applying a third 61 nm layer leads to a structure where the bottom two layers form the I-shaped structures and the top layer forms the inverted T structure (Figure 5a,b). Without the surface modification steps, the structure is poorly ordered and the cylinder orientations vary (Figure S3a,b).

These examples show that the inverted-T structure of a metallized 61 nm thick layer is converted to an I-shaped structure when an upper layer is coated and annealed on top;

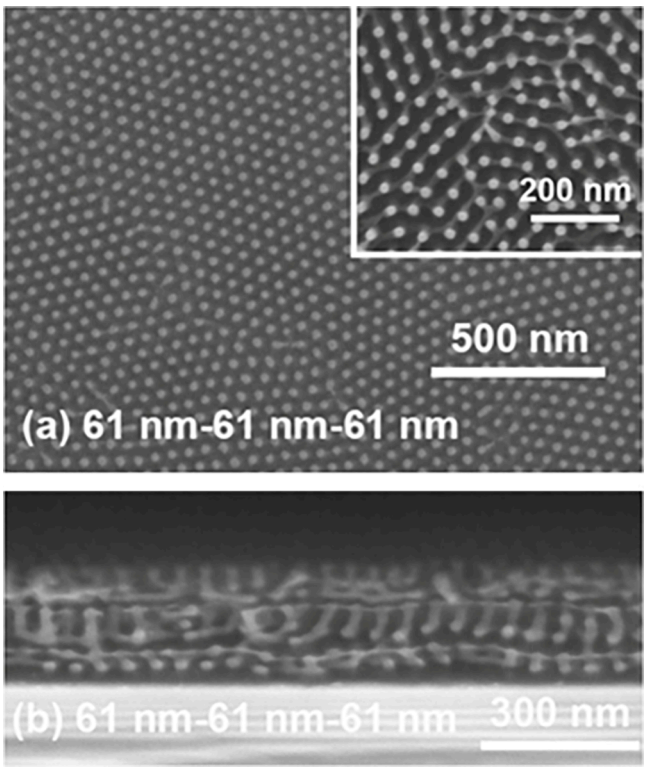

Figure 5. Morphology of three-layer metallized films. The films are prepared by spin coating a 61 nm layer of SV115, then annealing and metallization, and then repeating the following sequence twice: surface modification, coating a layer of 61 nm, annealing and metallization. (a) Top view with inset showing a sample after a longer etching time. (b) Cross section.

i.e., processing the second layer produces a bridging layer above the vertical cylinders of the first layer. To understand the mechanism for this morphology development, we examine the effects of spin-coating and annealing of a homo-PS layer (30 nm thick) on the 61 nm thick metalized inverted-T structure. The solvent annealing by itself has no effect on the metallized 61 nm layer (Figure S4a). However, application of the homo-PS layer leads to the formation of Pt-infiltrated cylinders parallel to the interface with homo-PS, connecting the vertical cylinders of the lower layer (Figure S4b). We describe this reorganization as "tip bending" because it reorients the tops of the vertical cylinders of the first layer into in-plane features. The PS top-coat layer is assumed to interdiffuse with the upper layer of the PS majority block and facilitate reorientation of the upper regions of the Pt-infiltrated P2VP microdomains, even though the mobility of the P2VP chains is reduced by the infiltrated metal. We hypothesize that a top layer of PS-*b*-P2VP BCP has a similar effect, forming in-plane cylinders that bridge the vertical cylinders and producing the I-shaped structures seen in Figure 4c,d.

Effects of Metal Exfiltration. The presence or absence of Pt in the P2VP microdomains of the first layer affects the morphology of the stacked films. A KOH + Na_2EDTA solution is used to remove metal from the P2VP microdomains, "unlocking" the microdomains and enabling annealing-induced changes to the morphology.[43] Once the metal is removed, the film can readily interdiffuse with a second film coated on top of it. For example, if a region of the metallized 37 nm thick film with in-plane cylinders is unlocked by removing the Pt, then a

https://doi.org/10.1021/acsapm.4c02331
ACS Appl. Polym. Mater. XXXX, XXX, XXX−XXX

second 37 nm layer is coated on top and annealed, the two layers merge to form an inverted-T structure (Figure S5a,c). This morphology is the same as that formed from a single-layer 74 nm thick film and differs from the orthogonal in-plane cylinder morphology found in the bilayer when the first layer is metallized (Figures 3,c and S1a,c). Similarly, coating a second 61 nm layer on a 61 nm layer from which the metal was removed leads to one inverted-T structure with longer out-of-plane cylinders (Figure S5b,d), instead of the I-shaped plus inverted-T structures shown in Figure 4b,d.

The short etch process used to modify the surface of the first layer prevents metal removal from unlocking the morphology. In other words, a process consisting of spin coating, annealing, metallization, surface modification, and unloading of a first layer and then spin coating, annealing, and metallization of a second layer produces the same final structure as if the unloading step had been omitted. The surface modification process removes some of the organic components from the top surface (Figure S7d,e)[36,54,55] and modifies the surface chemistry.[56−59] XPS results (Figure S8 and Table S1) show an increase in surface oxygen content (3.89% to 22.22%) and reduction in the ratios of C:O (1:0.05 to 1:0.32) and Cl:Pt (1:0.29 to 1:1.01) after surface modification, suggesting that both the polymer and the infiltrated metal are oxidized.

The surface oxidation and possible cross-linking caused by the surface modification process prevent reorganization of the microdomains during the processing of the second layer, even if an unloading step is used. This is illustrated further in Figure S6 which shows the structure of two layer films in which the first layer was annealed, metallized, surface modified, and then exfiltrated. This yields the same final structure as a process without the exfiltration step. For example, a 37 nm−37 nm film (Figure S6a,c) produced the same mesh structure as found without the unloading step (Figure 3a,c),[46] and a 61 nm−61 nm film (Figure S6b,d) produced the I-shaped structure in the first layer and inverted-T structure in the second layer, the same as Figure 3b,d. The significance of this result is that the surface modification etch process is readily applied to specific regions of the film by masking or lithography,[48,60,61] prior to a global exfiltration process, allowing local control of 3D morphologies within the film.

Interconnected in-plane and out-of-plane cylinders, including I-shaped structures and inverted-T structure, may be useful for the fabrication of metallization for integrated circuits and cross-point memory devices[4,26] and photovoltaic devices.[62,63] In addition to these interconnected structures, reversible metal infiltration achieves morphological and functional diversity in different regions, expanding the toolbox for nanofabrication.

CONCLUSIONS

This work demonstrates multilayer 3D structure design in PS-*b*-P2VP stacked thin films constructed by sequential layer-by-layer self-assembly. Two distinct processes have been identified to lock the structures in the bottom layer when another layer is coated and annealed, so that the layers form distinct 3D structures instead of merging to form a morphology characteristic of a single thicker layer. The first of these processes is a reversible metal infiltration process using an acid solution of a metal salt. Metal infiltration preserves the morphology of the lower layer of microdomains when a second layer is applied, although metallized vertical cylinders in the lower layer undergo tip bending, a reorganization of the top surface to produce in-plane bridging features, creating a I-shaped morphology. Unloading the metal by KOH + Na_2EDTA unlocks the structure of the bottom layer, which then merges with the upper layer to form inverted-T structures during a subsequent annealing process. The second process that locks the lower layer morphology is an (irreversible) surface modification using a short oxygen etch. Surface modification alters the chemical composition and topography of the metallized microdomains and locks the metallized microdomain structure even when a metal unloading process is carried out. By combining these methods, films with separate regions of multilayered structures and merged single-layer structures could be made by locally masking the surface, performing a surface modification etch, removing the mask, and then carrying out an unloading process over the entire surface. The surface-modified areas will form multilayer microdomains, whereas the masked areas will form merged structures. Etching-induced surface modification and reversible metal infiltration offer a suite of tools for creating 3D nanostructures from block copolymers.

ASSOCIATED CONTENT

Supporting Information

The Supporting Information is available free of charge at https://pubs.acs.org/doi/10.1021/acsapm.4c02331.

Figures of two-layer metallized films without surface modification, three-layer metallized films without surface modification, tip bending mechanism, merged films in unloaded regions of two-layer films, preserved structure in two-layer films after surface modification and unloading, topography of metallization-induced protrusions, and XPS analysis of surface modification (PDF)

AUTHOR INFORMATION

Corresponding Author

Caroline A. Ross − *Department of Materials Science and Engineering, Massachusetts Institute of Technology, Cambridge, Massachusetts 02139, United States;* orcid.org/0000-0003-2262-1249; Email: caross@mit.edu

Author

Mingchao Ma − *Department of Materials Science and Engineering, Massachusetts Institute of Technology, Cambridge, Massachusetts 02139, United States;* orcid.org/0000-0003-4563-7542

Complete contact information is available at: https://pubs.acs.org/10.1021/acsapm.4c02331

Notes

The authors declare no competing financial interest.

ACKNOWLEDGMENTS

We acknowledge a Postdoctoral Fellowship from Shanghai Jiao Tong University and support from NSF DMREF award 2118678.

REFERENCES

(1) Kim, S. O.; Solak, H. H.; Stoykovich, M. P.; Ferrier, N. J.; de Pablo, J. J.; Nealey, P. F. Epitaxial Self-assembly of Block Copolymers on Lithographically Defined Nanopatterned Substrates. *Nature* **2003**, *424*, 411−414.

(2) Ruiz, R.; Kang, H.; Detcheverry, F. A.; Dobisz, E.; Kercher, D. S.; Albrecht, T. R.; de Pablo, J. J.; Nealey, P. F. Density Multiplication and Improved Lithography by Directed Block Copolymer Assembly. *Science* **2008**, *321*, 936−939.
(3) Tang, C.; Lennon, E. M.; Fredrickson, G. H.; Kramer, E. J.; Hawker, C. J. Evolution of Block Copolymer Lithography to Highly Ordered Square Arrays. *Science* **2008**, *322*, 429−432.
(4) Tavakkoli, K. G. A.; Gotrik, K. W.; Hannon, A. F.; Alexander-Katz, A.; Ross, C. A.; Berggren, K. K. Templating Three-Dimensional Self-Assembled Structures in Bilayer Block Copolymer Films. *Science* **2012**, *336*, 1294−1298.
(5) Darling, S. B. Directing the self-assembly of block copolymers. *Prog. Polym. Sci.* **2007**, *32*, 1152−1204.
(6) Kim, H.-C.; Hinsberg, W. D. Surface Patterns from Block Copolymer Self-assembly. *J. Vac. Sci. Technol. A* **2008**, *26*, 1369−1382.
(7) Kim, J. K.; Yang, S. Y.; Lee, Y.; Kim, Y. Functional Nanomaterials Based on Block Copolymer Self-assembly. *Prog. Polym. Sci.* **2010**, *35*, 1325−1349.
(8) Brassat, K.; Kool, D.; Bürger, J.; Lindner, J. K. N. Hierarchical nanopores formed by block copolymer lithography on the surfaces of different materials pre-patterned by nanosphere lithography. *Nanoscale* **2018**, *10*, 10005−10017.
(9) Han, E.; Stuen, K. O.; Leolukman, M.; Liu, C.-C.; Nealey, P. F.; Gopalan, P. Perpendicular Orientation of Domains in Cylinder-Forming Block Copolymer Thick Films by Controlled Interfacial Interactions. *Macromolecules* **2009**, *42*, 4896−4901.
(10) Pang, Y.; Wan, L.; Huang, G.; Zhang, X.; Jin, X.; Xu, P.; Liu, Y.; Han, M.; Wu, G.-P.; Ji, S. Controlling Block Copolymer-Substrate Interactions by Homopolymer Brushes/Mats. *Macromolecules* **2017**, *50*, 6733−6741.
(11) Mocan, M.; Kamperman, M. Self-assembly of PS-b-PNIPAM-b-PS block copolymer thin films via selective solvent annealing. *Polymer* **2016**, *107*, 387−397.
(12) Chavis, M. A.; Smilgies, D.-M.; Wiesner, U. B.; Ober, C. K. Widely Tunable Morphologies in Block Copolymer Thin Films Through Solvent Vapor Annealing Using Mixtures of Selective Solvents. *Adv. Funct. Mater.* **2015**, *25*, 3057−3065.
(13) Jung, Y. S.; Ross, C. A. Solvent-Vapor-Induced Tunability of Self-Assembled Block Copolymer Patterns. *Adv. Mater.* **2009**, *21*, 2540−2545.
(14) Shi, L.-Y.; Yin, C.; Zhou, B.; Xia, W.; Weng, L.; Ross, C. A. Annealing Process Dependence of the Self-Assembly of Rod-Coil Block Copolymer Thin Films. *Macromolecules* **2021**, *54*, 1657−1664.
(15) Jin, H. M.; Park, D. Y.; Jeong, S.-J.; Lee, G. Y.; Kim, J. Y.; Mun, J. H.; Cha, S. K.; Lim, J.; Kim, J. S.; Kim, K. H.; Lee, K. J.; Kim, S. O. Flash Light Millisecond Self-Assembly of High χ Block Copolymers for Wafer-Scale Sub-10 nm Nanopatterning. *Adv. Mater.* **2017**, *29*, 1700595.
(16) Yang, G. G.; Choi, H. J.; Li, S.; Kim, J. H.; Kwon, K.; Jin, H. M.; Kim, B. H.; Kim, S. O. Intelligent block copolymer self-assembly towards IoT hardware components. *Nat. Rev. Electr. Eng.* **2024**, *1*, 124−138.
(17) Brassat, K.; Kool, D.; Nallet, C. G. A.; Lindner, J. K. N. Understanding Film Thickness-Dependent Block Copolymer Self-Assembly by Controlled Polymer Dewetting on Prepatterned Surfaces. *Adv. Mater. Interfaces* **2020**, *7*, 1901605.
(18) Lee, W.; Lee, S.; Tang, A. S.; Kim, C.; Liu, R.; Im, K.; Jung, H.-T.; Ross, C. A. Platinum Infiltration of a Block Copolymer for Interconnected Three-Dimensional Metal Nanostructures. *ACS Appl. Nano Mater.* **2021**, *4*, 793−801.
(19) Bai, W.; Yager, K. G.; Ross, C. A. In Situ Characterization of the Self-Assembly of a Polystyrene-Polydimethylsiloxane Block Copolymer during Solvent Vapor Annealing. *Macromolecules* **2015**, *48*, 8574−8584.
(20) Cheng, J. Y.; Ross, C. A.; Thomas, E. L.; Smith, H. I.; Vancso, G. J. Templated Self-Assembly of Block Copolymers: Effect of Substrate Topography. *Adv. Mater.* **2003**, *15*, 1599−1602.
(21) Jung, Y. S.; Jung, W.; Ross, C. A. Nanofabricated Concentric Ring Structures by Templated Self-Assembly of a Diblock Copolymer. *Nano Lett.* **2008**, *8*, 2975−2981.
(22) Ruiz, R.; Ruiz, N.; Zhang, Y.; Sandstrom, R. L.; Black, C. T. Local Defectivity Control of 2D Self-Assembled Block Copolymer Patterns. *Adv. Mater.* **2007**, *19*, 2157−2162.
(23) Bita, I.; Yang, J. K. W.; Jung, Y. S.; Ross, C. A.; Thomas, E. L.; Berggren, K. K. Graphoepitaxy of Self-Assembled Block Copolymers on Two-Dimensional Periodic Patterned Templates. *Science* **2008**, *321*, 939−943.
(24) Park, S.; Lee, D. H.; Xu, J.; Kim, B.; Hong, S. W.; Jeong, U.; Xu, T.; Russell, T. P. Macroscopic 10-Terabit-per-Square-Inch Arrays from Block Copolymers with Lateral Order. *Science* **2009**, *323*, 1030−1033.
(25) Ludwigs, S.; Böker, A.; Voronov, A.; Rehse, N.; Magerle, R.; Krausch, G. Self-assembly of functional nanostructures from ABC triblock copolymers. *Nat. Mater.* **2003**, *2*, 744−747.
(26) Yang, J. K. W.; Jung, Y. S.; Chang, J.-B.; Mickiewicz, R. A.; Alexander-Katz, A.; Ross, C. A.; Berggren, K. K. Complex self-assembled patterns using sparse commensurate templates with locally varying motifs. *Nat. Nanotechnol.* **2010**, *5*, 256−260.
(27) Crossland, E. J. W.; Kamperman, M.; Nedelcu, M.; Ducati, C.; Wiesner, U.; Smilgies, D.-M.; Toombes, G. E. S.; Hillmyer, M. A.; Ludwigs, S.; Steiner, U.; Snaith, H. J. A Bicontinuous Double Gyroid Hybrid Solar Cell. *Nano Lett.* **2009**, *9*, 2807−2812.
(28) Crossland, E. J. W.; Ludwigs, S.; Hillmyer, M. A.; Steiner, U. Control of gyroid forming block copolymer templates: effects of an electric field and surface topography. *Soft Matter* **2010**, *6*, 670−676.
(29) Hsueh, H.-Y.; Huang, Y.-C.; Ho, R.-M.; Lai, C.-H.; Makida, T.; Hasegawa, H. Nanoporous Gyroid Nickel from Block Copolymer Templates via Electroless Plating. *Adv. Mater.* **2011**, *23*, 3041−3046.
(30) Hsueh, H.-Y.; Chen, H.-Y.; She, M.-S.; Chen, C.-K.; Ho, R.-M.; Gwo, S.; Hasegawa, H.; Thomas, E. L. Inorganic Gyroid with Exceptionally Low Refractive Index from Block Copolymer Templating. *Nano Lett.* **2010**, *10*, 4994−5000.
(31) Wang, X.-B.; Lo, T.-Y.; Hsueh, H.-Y.; Ho, R.-M. Double and Single Network Phases in Polystyrene-*block*-poly(L-lactide) Diblock Copolymers. *Macromolecules* **2013**, *46*, 2997−3004.
(32) Rose, F.; Bosworth, J. K.; Dobisz, E. A.; Ruiz, R. Three-dimensional mesoporous structures fabricated by independent stacking of self-assembled films on suspended membranes. *Nanotechnology* **2011**, *22*, No. 035603.
(33) Oh, J.; Suh, H. S.; Ko, Y.; Nah, Y.; Lee, J.-C.; Yeom, B.; Char, K.; Ross, C. A.; Son, J. G. Universal Perpendicular Orientation of Block Copolymer Microdomains Using a Filtered Plasma. *Nat. Commun.* **2019**, *10*, 2912.
(34) Kuila, B. K.; Formanek, P.; Stamm, M. Multilayer polymer thin films for fabrication of ordered multifunctional polymer nanocomposites. *Nanoscale* **2013**, *5*, 10849−10852.
(35) Kim, S. Y.; Nunns, A.; Gwyther, J.; Davis, R. L.; Manners, I.; Chaikin, P. M.; Register, R. A. Large-Area Nanosquare Arrays from Shear-Aligned Block Copolymer Thin Films. *Nano Lett.* **2014**, *14*, 5698−5705.
(36) Chai, J.; Wang, D.; Fan, X.; Buriak, J. M. Assembly of aligned linear metallic patterns on silicon. *Nat. Nanotechnol.* **2007**, *2*, 500−506.
(37) Kim, J. J.; Suh, H. S.; Zhou, C.; Mane, A. U.; Lee, B.; Kim, S.; Emery, J. D.; Elam, J. W.; Nealey, P. F.; Fenter, P.; Fister, T. T. Mechanistic Understanding of Tungsten Xxide In-plane Nanostructure Growth via Sequential Infiltration Synthesis. *Nanoscale* **2018**, *10*, 3469−3479.
(38) Shin, D. O.; Lee, D. H.; Moon, H.-S.; Jeong, S.-J.; Kim, J. Y.; Mun, J. H.; Cho, H.; Park, S.; Kim, S. O. Sub-Nanometer Level Size Tuning of a Monodisperse Nanoparticle Array Via Block Copolymer Lithography. *Adv. Funct. Mater.* **2011**, *21*, 250−254.
(39) Wu, N. L. Y.; Zhang, X.; Murphy, J. N.; Chai, J.; Harris, K. D.; Buriak, J. M. Density Doubling of Block Copolymer Templated Features. *Nano Lett.* **2012**, *12*, 264−268.

https://doi.org/10.1021/acsapm.4c02331
ACS Appl. Polym. Mater. XXXX, XXX, XXX−XXX

(40) Aizawa, M.; Buriak, J. M. Block Copolymer Templated Chemistry for the Formation of Metallic Nanoparticle Arrays on Semiconductor Surfaces. *Chem. Mater.* **2007**, *19*, 5090−5101.
(41) Chai, J.; Buriak, J. M. Using Cylindrical Domains of Block Copolymers To Self-Assemble and Align Metallic Nanowires. *ACS Nano* **2008**, *2*, 489−501.
(42) Cummins, C.; Gangnaik, A.; Kelly, R. A.; Borah, D.; O'Connell, J.; Petkov, N.; Georgiev, Y. M.; Holmes, J. D.; Morris, M. A. Aligned silicon nanofins via the directed selfassembly of PS-b-P4VP block copolymer and metal oxide enhanced pattern transfer. *Nanoscale* **2015**, *7*, 6712−6721.
(43) Ma, M.; Liu, R.; Su, T.; Sun, Z.; Ross, C. A. Reversible Morphology Locking via Metal Infiltration in a Block Copolymer. *ACS Nano* **2023**, *17*, 12225−12233.
(44) Subramanian, A.; Tiwale, N.; Doerk, G.; Kisslinger, K.; Nam, C.-Y. Enhanced Hybridization and Nanopatterning via Heated Liquid-Phase Infiltration into Self-Assembled Block Copolymer Thin Films. *ACS Appl. Mater. Interfaces* **2020**, *12*, 1444−1453.
(45) Majewski, P. W.; Rahman, A.; Black, C. T.; Yager, K. G. Arbitrary lattice symmetries via block copolymer nanomeshes. *Nat. Commun.* **2015**, *6*, 7448.
(46) Liu, R.; Huang, H.; Sun, Z.; Alexander-Katz, A.; Ross, C. A. Metallic Nanomeshes Fabricated by Multimechanism Directed Self-Assembly. *ACS Nano* **2021**, *15*, 16266−16276.
(47) Shin, D. O.; Mun, J. H.; Hwang, G.-T.; Yoon, J. M.; Kim, J. Y.; Yun, J. M.; Yang, Y.-B.; Oh, Y.; Lee, J. Y.; Shin, J.; Lee, K. J.; Park, S.; Kim, J. U.; Kim, S. O. Multicomponent Nanopatterns by Directed Block Copolymer Self-Assembly. *ACS Nano* **2013**, *7*, 8899−8907.
(48) Mun, J. H.; Cha, S. K.; Kim, Y. C.; Yun, T.; Choi, Y. J.; Jin, H. M.; Lee, J. E.; Jeon, H. U.; Kim, S. Y.; Kim, S. O. Controlled Segmentation of Metal Nanowire Array by Block Copolymer Lithography and Reversible Ion Loading. *Small* **2017**, *13*, 1603939.
(49) Mieczkowski, R. The Determination of the Solubility Parameter Components of Polystyrene. *Eur. Polym. J.* **1989**, *25*, 1055−1057.
(50) Arras, M. M. L.; He, B.; Jandt, K. D. High molar mass amphiphilic block copolymer enables alignment and dispersion of unfunctionalized carbon nanotubes in melt-drawn thin-films. *Polymer* **2017**, *127*, 15−27.
(51) Kim, S. H.; Misner, M. J.; Xu, T.; Kimura, M.; Russell, T. P. Highly Oriented and Ordered Arrays from Block Copolymers via Solvent Evaporation. *Adv. Mater.* **2004**, *16*, 226−231.
(52) Huang, H.; Liu, R.; Ross, C. A.; Alexander-Katz, A. Self-Directed Self-Assembly of 3D Tailored Block Copolymer Nanostructures. *ACS Nano* **2020**, *14*, 15182−15192.
(53) Amir Tavakkoli, K. G.; Nicaise, S. M.; Gadelrab, K. R.; Alexander-Katz, A.; Ross, C. A.; Berggren, K. K. Multilayer block copolymer meshes by orthogonal self-assembly. *Nat. Commun.* **2016**, *7*, 10518.
(54) Xiong, S.; Wan, L.; Ishida, Y.; Chapuis, Y.-A.; Craig, G. S. W.; Ruiz, R.; Nealey, P. F. Directed Self-Assembly of Triblock Copolymer on Chemical Patterns for Sub-10-nm NanofabricationviaSolvent Annealing. *ACS Nano* **2016**, *10*, 7855−7865.
(55) Mun, J. H.; Cha, S. K.; Kim, H.; Moon, H.-S.; Kim, J. Y.; Jin, H. M.; Choi, Y. J.; Baek, J. E.; Shin, J.; Kim, S. O. Nanodomain Swelling Block Copolymer Lithography for Morphology Tunable Metal Nanopatterning. *Small* **2014**, *10*, 3742−3749.
(56) Chen, Y.; Gao, Q.; Wan, H.; Yi, J.; Wei, Y.; Liu, P. Surface modification and biocompatible improvement of polystyrene film by Ar, O2 and Ar + O2 plasma. *Appl. Surf. Sci.* **2013**, *265*, 452−457.
(57) Vesel, A.; Mozetic, M. Surface modification and ageing of PMMA polymer by oxygen plasma treatment. *Vacuum* **2012**, *86*, 634−637.
(58) Vesel, A.; Junkar, I.; Cvelbar, U.; Kovac, J.; Mozetic, M. Surface modification of polyester by oxygen-and nitrogen-plasma treatment. *Surf. Interface Anal.* **2008**, *40*, 1444−1453.
(59) Murakami, T.; Kuroda, S.-i.; Osawa, Z. Dynamics of Polymeric Solid Surfaces Treated with Oxygen Plasma: Effect of Aging Media after Plasma Treatment. *J. Colloid Interface Sci.* **1998**, *202*, 37−44.
(60) Liu, C.-C.; Nealey, P. F.; Raub, A. K.; Hakeem, P. J.; Brueck, S. R. J.; Han, E.; Gopalan, P. Integration of block copolymer directed assembly with 193 immersion lithography. *J. Vac. Sci. Technol. B* **2010**, *28*, C6B30−C6B34.
(61) Farrell, R. A.; Kinahan, N. T.; Hansel, S.; Stuen, K. O.; Petkov, N.; Shaw, M. T.; West, L. E.; Djara, V.; Dunne, R. J.; Varona, O. G.; Gleeson, P. G.; Jung, S.-J.; Kim, H.-Y.; Koleśnik, M. M.; Lutz, T.; Murray, C. P.; Holmes, J. D.; Nealey, P. F.; Duesberg, G. S.; Krstić, V.; Morris, M. A. Large-scale parallel arrays of silicon nanowires via block copolymer directed self-assembly. *Nanoscale* **2012**, *4*, 3228−3236.
(62) Tan, K. W.; Moore, D. T.; Saliba, M.; Sai, H.; Estroff, L. A.; Hanrath, T.; Snaith, H. J.; Wiesner, U. Thermally Induced Structural Evolution and Performance of Mesoporous Block CopolymerDirected Alumina Perovskite Solar Cells. *ACS Nano* **2014**, *8*, 4730−4739.
(63) Li, C.; Li, Q.; Kaneti, Y. V.; Hou, D.; Yamauchi, Y.; Mai, Y. Self-assembly of block copolymers towards mesoporous materials for energy storage and conversion systems. *Chem. Soc. Rev.* **2020**, *49*, 4681−4736.

https://doi.org/10.1021/acsapm.4c02331
ACS Appl. Polym. Mater. XXXX, XXX, XXX−XXX